

Ethanol electro-oxidation on Pt/CNFs-GNPs/GDL electrode for fuel cell application

Maryam Yaldagard ^{1,*}

¹Department of Chemical Engineering, Urmia University, Iran

Article Information

Article History:

Received:

6 Jun 2022

Received in revised form:

6 Jul 2022

Accepted:

26 Jul 2022

Keywords

Ethanol electro-oxidation
electrodeposition

CNF

GNP

fuel cell

Abstract

Among direct alcohol fuel cells, the ethanol fuel cell is considered the most acceptable in terms of safety and power density. In this research, a Pt/CNFs-GNPs/GDL electrode was developed using GNPs and CNFs as a supporting medium on carbon paper and the electrodeposition method to deposit Pt catalyst. The morphology and structure features of the prepared film samples were characterized by FESEM and XRD. Pt particles of about 6.53 nm were uniformly deposited on the porous support. Catalytic activities of the prepared electrode for the ethanol oxidation reaction were evaluated through cyclic voltammetry measurements. Based on the electrochemical properties, the as-prepared Pt/CNFs-GNPs/GDL electrocatalyst exhibited a comparable activity for ethanol oxidation reaction for the Pt/C, which may be attributed to the high specific surface area of the CNFs support as well as high conductivity of graphene nanoplates. A notable reduction in the onset and peak potential of ethanol electro-oxidation from 0.55 and 0.81V for Pt/C/GDL to 0.50 and 0.79V for Pt/CNFs-GNPs/GDL electrodes, as well as a substantial increment in anodic Tafel slope values from 376 mV to 521 mV, indicates that an increase in the activity for EOR is achieved by replacing C with CNFs-GNPs.

1. Introduction

In recent years, direct alcohol fuel cells (DAFCs) have been attracting more and more attention as an alternative to conventional internal combustion engines due to their potential applications in transportation and portable electronic devices. DAFCs use methanol or ethanol directly as fuel without an external reformer,

which makes it simple and compact. Compared with methanol, ethanol has more energy density [1]. In addition, ethanol presents lower toxicity, price, and a decreased crossover effect through solid electrolytes [2-4], so it is safer and can be produced in large quantities from biomass fermentation. Hence, ethanol is a more attractive fuel than methanol for DAFCs despite its low electro-oxidation kinetics due to the difficulties in

*Corresponding Author: m.yaldagard@urmia.ac.ir
m_yaldagard@yahoo.com Tel: +98-4432775660

breaking the C-C bond and complete oxidation to CO₂ [5, 6]. Due to DAFCs efficiency's strong dependence on the catalyst layer, catalysts-supporting strategies have been developed. Carbon black is usually used as the catalyst support because of its large surface area (which elevates its metal dispersion), pore structure (which facilitates the transport of reactant gases), and high electrical conductivity [1]. However, there are some disadvantages related to using carbon black, such as corrosion of the carbon surface in the fuel cell environment, which can cause fuel cell performance losses. On this basis, various alternative catalyst supports, such as nanostructured conductive carbon materials and a composite of these materials, have been studied to minimize the use of precious metals and improve the stability and catalytic activity of the catalyst [7]. Nanostructured carbon materials such as graphite nanofibers (CNFs) [8, 9] and graphene nanoplates (GNPs) [10-12] have been successfully used as catalyst support in direct alcohol fuel cells. They also improved oxidation activities of the catalyst compared to a Vulcan carbon catalyst support in the above mentioned studies [8-12] due to their good electronic conductivity, high surface area, and chemical stability. The CNF nanostructures consist of graphite sheets aligned in specific directions dictated by the catalytic entity selected for the growth process. The unique properties of carbon nanofibers (CNFs), sometimes called carbon filaments, have generated intense interest in their use for a number of applications, including selective absorption, energy storage, polymer reinforcement, and catalyst supports [13]. Unlike conventional graphite materials and nanotubes where the basal plane is exposed, the structure of carbon nanofibers is such that only edge regions are exposed [13]. This feature allows CNFs to be used as a catalyst support for fuel cells. Generally, CNFs have a high specific surface area with shallow pores, resulting in enhanced electrochemical activity. Although CNFs have a high specific surface area, the low conductivity of porous carbon materials has limited their application in cat-

alyst supports [14, 15]. Some literature reported that the introduction of graphene into a carbon matrix experimentally improved the electric conductivity as well as the mechanical properties of the original carbon matrix [16-18]. In addition, CNF and graphene oxide sheets can be stably dispersed in water due to their hydrophilic nature [16, 19]. Furthermore, CNF has a strong and attractive interaction with graphene oxide via hydrogen bonding and van der Waals interaction [20].

Graphene nano platelets (GNPs), typically consisting of single to few-layer sheets of sp²-hybridized carbon atoms forming two-dimensional layers with a thickness in the nanometer scale, possess attractive characteristics such as high electrical conductivity, high modulus, high charge transfer capacity, and high specific surface area [21, 22]. As compared to chemical vapor deposition (CVD) grown carbon nanotubes (CNTs), the graphene platelets are comparatively cheaper. Because of their unique structural, mechanical, and electronic properties, graphene nanoplates are currently attracting enormous interest in nanoelectronics, sensors, nanocomposites, batteries, supercapacitors, and hydrogen storage. In particular, graphene has potential application as a catalyst support in PEM fuel cells owing to have high surface areas (theoretical specific surface area of 2620m²g⁻¹) and high conductivity [12, 23]. Graphene-supported Pt or Pt-Ru nanoparticles displayed excellent electrocatalytic activity for methanol and ethanol oxidation [12, 23-26].

This study focuses on the electrodeposition of Pt on the composite support of CNFs and GNPs in the gas diffusion layer. Ethanol electro oxidation was investigated on a prepared Pt/CNFs-GNPs/GDL electrode.

2. Experimental

2.1. Materials

High-purity graphite powder (99.9999%, 200 mesh)

was purchased from Alfa Aesar. Chemicals $\text{H}_2\text{PtCl}_6 \cdot 6\text{H}_2\text{O}$ (40 %), hydrazine hydrate, sodium nitrate, KMnO_4 , H_2O_2 , and CNFs were obtained from Sigma-Aldrich. All solvents, including H_2SO_4 , 2-propanol, and Triton X100, were used as received from Sigma-Aldrich without further purification. Nafion® solution (Ion power Inc., USA 5 wt %), carbon cloth (Teflon treated), and Pt/C (20 wt %) were bought from the Fuel Cell Earth Company. High purified N_2 (99.9995 %) gas was purchased from Canadian Sigma. Inc. Water purified by a Milli-Q water purification system was used throughout the electrodeposition experimental work.

2.2. Methods

2.2.1. Chemical Preparation of Graphene Oxide (GO) and GNPs

Chemical preparation of graphene oxide (GO) and GNPs was done according to our previously published papers [27, 28]. In a typical synthesis process, natural graphite powder was oxidized to graphite oxide by a modified Hummers and Offenman's method [29]. In brief, 2 g graphite powder and 1g sodium nitrate were transferred into 90ml concentrated H_2SO_4 in ice bath conditions. Then, 6 g KMnO_4 was regularly added. The mixture was stirred at $35 \pm 5^\circ\text{C}$ for 8 h. Then 200 ml of deionized water (DI) was added. Next, the solution was diluted with 400ml DI. Following that, 5 % H_2O_2 was added into the solution until the color of the mixture altered from brown to peril yellow. The solution was then filtrated via vacuum büchner filtration, and the filter cake was dispersed in DI by means of an ultrasonic bath. The mixture was washed with 1:20 HCL solution and water by repeated centrifugation at 11000 rpm for 20 min to a pH value of 7 and dried in a vacuum oven at 60°C for 24h. The obtained graphite oxide was dispersed in DI water and exfo-

liated to generate graphene oxide by ultrasonication using a sonifier (UP400S, 80amplitude). The brown graphene oxide nanoplates dispersion was transferred into a round-bottomed flask, to which hydrazine monohydrate (as a reducing agent) was added. The mixed solution was then refluxed at 100°C for 2h, during which the color of the solution gradually changed dark black as the graphene nanosheets dispersion floating at the air/solution interface of the dispersion was formed. The dispersion was further centrifuged for 15 min at 3000 rpm to remove a small amount of precipitate. Finally, the supernatant of the graphene nanosheets dispersion was directly dried in a vacuum oven to obtain the bulk of graphene nanosheet powders.

2.2.2 Preparation of nanocomposite of GNP and CNF

CNFs-GNPs mixed powders were produced using a pressure filtration method. A mixture of GNPs and CNFs (w/w, 1:3) in 1000 mL deionized water was sonicated to achieve a homogenous dispersion by adding Triton-X as a surfactant. The suspension was then filtered under N_2 pressure through a homemade nanofilter. The sediment was washed thoroughly with isopropanol to remove the residual surfactant. After drying, a thin film layer was peeled from the nanofilter to produce a composite system of CNFs-GNPs [30]. This unique design strategy not only provides a highly conductive network for CNFs-GNPs surface, but also maintains the structural integrity of CNFs [31].

2.2.3 Preparation of electrode of CNFs-GNPs / GDL and Electrodepositions of Pt Nanoparticles

To prepare the CNFs-GNPs base on the gas diffusion layer electrode, a suspension of the composite CNFs-GNPs system in ethanol/DI water was prepared

with the aid of an ultrasonic bath cleaner for 15 min. Then, 100 μ L of the prepared mixture was pipetted on carbon paper and dried at room temperature. The side of the electrode with the dried suspension was exposed to the electrolyte, and a cu wire was used to make electrical contact with the other sides. Electrodeposition was performed in a plating bath containing a solution of 4 mM $H_2PtCl_6 \cdot 6H_2O$ in 0.5 M NaCl. Before the Pt deposition, the active side of the porous carbon paper containing the composite of CNFs-GNPs was impregnated with a solution of 0.05% Nafion in ethanol. Following the deposition, the electrode was removed im-

mediately from the electrolyte, rinsed thoroughly with deionized water and dried in air [32]. A schematic of the experimental procedures used in this study for the preparation of Pt/CNFs-GNPs/GDL is illustrated in Fig. 1. The peak current density was 300 mAcm⁻² with an on/off time of 10/100 ms. Total amount of charge was 350 mCcm⁻² (Fig. 2). For comparison, the conventional Pt/C electrode was fabricated by spraying the catalyst slurry (commercial Pt/C (20 wt %, fuel cell earth company) nanoparticles in the ink preparation route with a loading of 1mgcm⁻² on carbon paper.

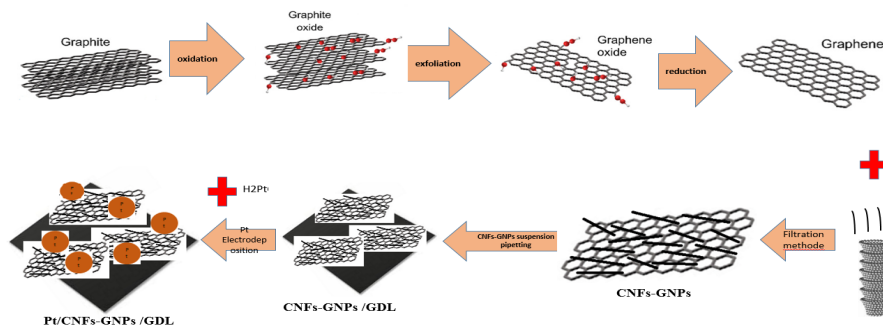


Fig. 1. A schematic of the experimental procedures used to prepare Pt/ CNFs-GNPs /GDL.

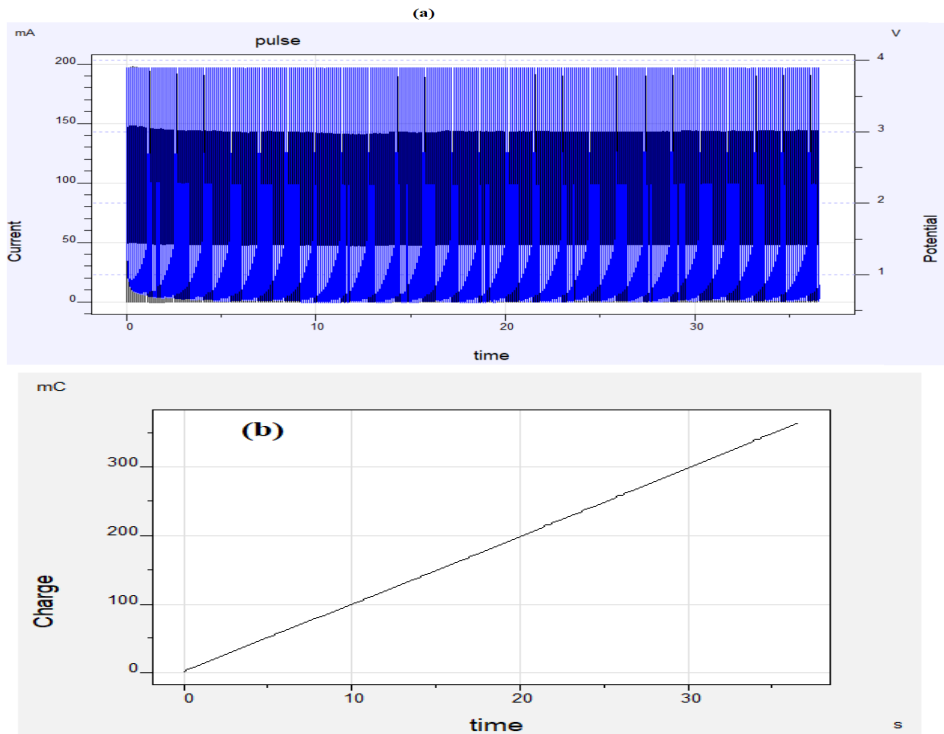


Fig. 2. (a) Presentation of the $i(v)$ - t plots of the Pt/CNFs-GNP/GDL electrode under electrodeposition. (b) The quantity of Pt deposited on the substrate.

2.3. Characterization

The samples for Raman spectroscopy were obtained by dropping a suspension of CNFs and GNPs onto the quartz cuvettes and then air drying to form a film. The measurements were performed from 500 to 3500 cm^{-1} at room temperature using a dispersive Raman microscope (Model: SENTERRA (2009) BRUKER (Germany)) with a Laser wave number of 785 nm.

The adsorption properties were used to analyze the characteristics, i.e., Brunauer-Emmett-Teller (BET) specific surface area, pore volume, and pore size distributions of graphene nanoplates. The cold bath temperature (77.3 K) N_2 adsorption was recorded using a PHS-1020(PHSCHINA) adsorption analyzer. Prior to the measurements, the sample was pretreated by out gassing in a vacuum oven at about 200°C for 10 h. The relative pressure was $0 < \frac{P}{P_0} < 0.4$

Further morphology and structure study of the graphene sheets, CNFs, and composite system was conducted by an atomic force microscope (AFM, model Nanosurf easy scan2) using contact mode. Field emission-scanning electron microscopy (FE-SEM) characterization and Energy dispersive X-ray (EDX) spectroscopy coupled to a scanning electron microscopy SEM MAG100.00kx with a silicon detector was performed at 15 KV.

The crystal structure of the catalyst was measured by X-ray diffraction XRD at room temperature with an X'Pert Pro MPD model (PANalytical) Diffractometer using Cu K ($\lambda = 0.15406 \text{ nm}$) radiation generated at 40KV and 40 mA with high resolution (0.001°). The 2θ angular regions between 10° and 90° were recorded with a step size of 0.039 (at a scan step time of 108.12s) with continuous scanning. The phase analysis was conduct-

ed by X'Pert Highscore Plus software from a thin film. Pt electrodeposition, EOR experiments, and all electrochemical measurements were carried out using a potentiostat/galvanostat model Iviumstat-XR electrochemical Interface System.

3. Result and discussion

3.1 Physical Characterization

3.1.1 Topography/Morphology and Structural Characterization of CNFs, Chemically Reduced Graphene Nanoplates, Composite System of CNFs-GNPs, and Electrodeposited Pt on CNFs-GNPs /Carbon based Electrode

The raw CNFs, chemically prepared graphene nanoplates, and obtained composites of graphene nanoplates on the CNF surfaces were analyzed by Atomic Force Microscopy (AFM) to determine their thickness and lateral size. Fig. 3 shows an AFM image of the above-mentioned materials with their corresponding height profile. The zoomed image of graphene nanoplates and corresponding line scan are shown in Fig. 3b. From this figure, we see the topographic height of the graphene nanoplates was about 19-156.2 nm, indicating a few-layered graphene nanoplates. In addition, the white areas depict the highest points on the surface, the dark orange regions are the lowest points on the surface, and the yellow areas are the levels between the highest and lowest regions.

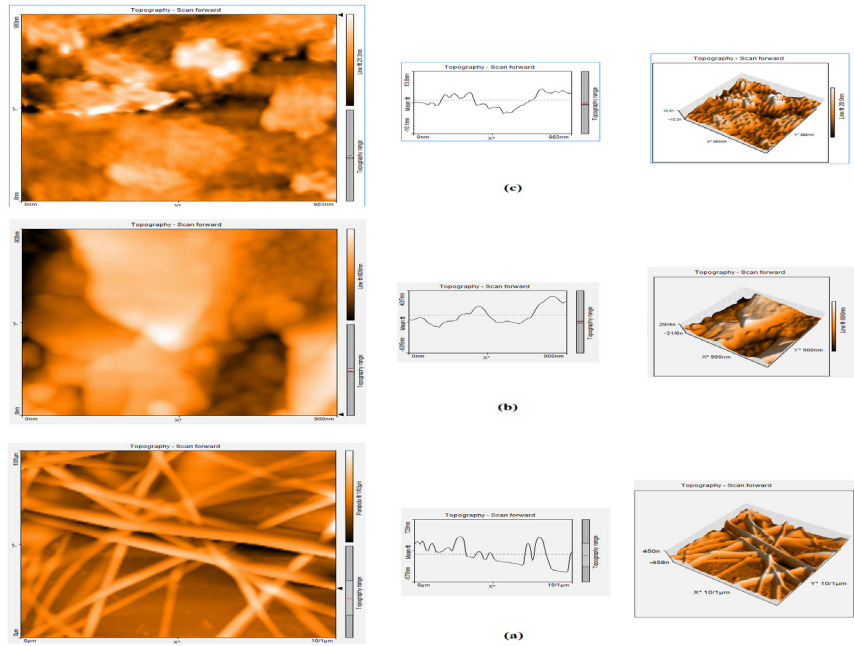


Fig. 3. AFM topography images of (a) CNFs, (b) graphene nanoplates, and (c) CNFs-GNPs nanoplates. Next to the images are a line scan taken horizontally through the image as marked with an arrow, from which the height of the graphene nanoplates and CNFs were determined.

The microstructures of the electrode were investigated by FESEM. The image (Fig. 4) shows that the large CNFs entangle to form a backbone, where a fine

meshwork of much smaller GNPs creates the surface covering layer. Well-dispersed Pt nanoparticles were observed on the support.

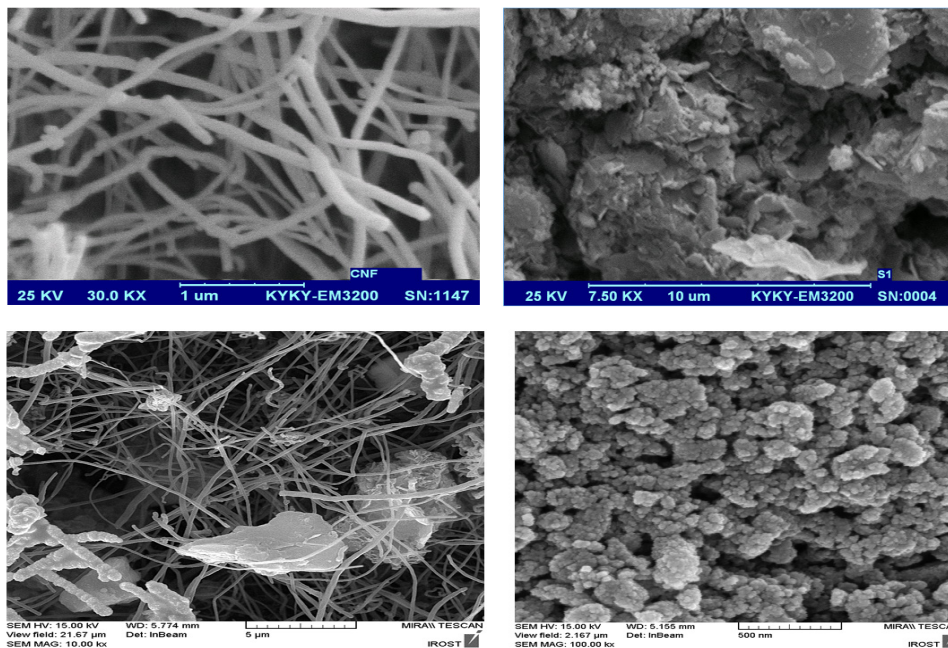


Fig. 4. (a) FESEM images of the CNF, (b) GNPs, (c) Pt/CNFs-GNPs/GDL composite, and (d) High resolution of Pt nanoparticles deposition on the substrate.

Fig. 5 shows the typical EDS pattern of the Pt/CN-Fs-GNPs/GDL electrode. It turns out that the prepared electrode contains Pt elements. The EDS pattern showed that C, O, and F are the major element of spectra. The C signal comes from the GNPs, CNFs, and Nafion solution. Oxygen and S are also derived from Nafion. A small part of the oxygen may be orig-

inated from the incomplete reduction of graphene oxide to graphene. Besides Pt, O, and C, the element of Si and Au were also detected. The strong peak of Si is due to the silicon substrate used in the FESEM analysis. The element Au belongs to the Au target from the sputtering chamber in FESEM characterization.

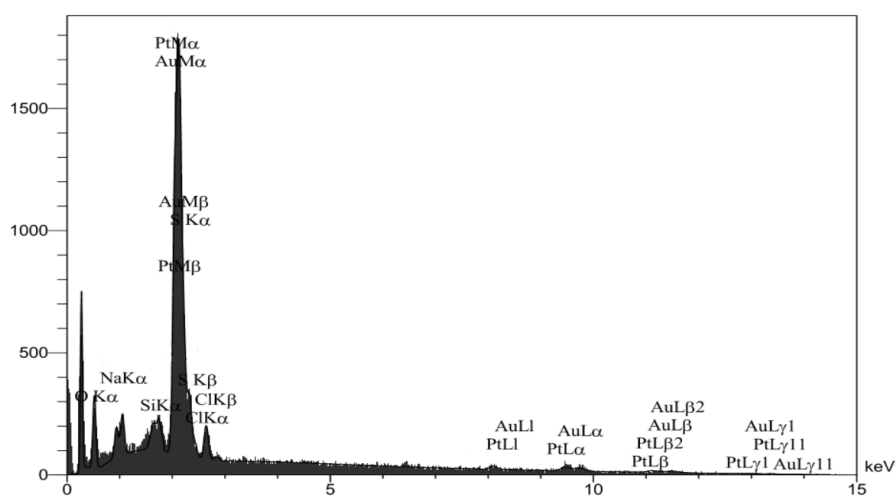


Fig. 5. EDX pattern of the Pt/CNFs-GNPs electrocatalyst.

Raman's spectroscopy is a useful tool to characterize graphitic materials, especially for distinguishing graphene and graphene oxide. It is a non-destructive technique that provides detailed structure information such as graphene disorder and defect structures [33]. The Raman spectrum of graphene is characterized by three main features caused by a change in electron bands: the G mode is related to the vibration of sp^2 -bonded carbon atoms in the two-dimensional hexagonal lattice (usually observed at about 1575 cm^{-1}); the D mode arising from the doubly resonant disorder-induced mode and related to defects (about 1350), and the symmetry-allowed 2D overtone mode (about 2700) bond is found at almost double the frequency of the D band and originates from the second order Raman scattering process [34-41]. As the structure changes from graphite to nanocrystalline graphene in graphene studies, the ratio between the peak intensity of the D and G line, I_D/I_G , changes inversely with the size of the crystalline grains or inter-defect distance

[42]. The higher I_D/I_G intensity ratio of a sample can be used as evidence for the structure order. Fig. 6 shows the typical Raman spectra of CNFs, graphene nanoplates, and CNFs-GNPs. CNFs display two prominent peaks, which correspond to the well-documented G and D bands, the first originates from the graphite structure of carbon and the second from the amorphous structure of carbon. The GNPs display three main featured peaks, namely G-band, D-band, and 2D band in 1585.66 cm^{-1} , 1311.30 cm^{-1} and 2611.92 cm^{-1} respectively. For GNPs, the G band appeared in 1585 cm^{-1} , which is close to the value of pristine graphite, confirming the reduction of graphene oxide by chemical reduction. The I_D/I_G ratios for GNP are about 1.65, which are higher than CNFs (about 0.83) and CNFs-GNPs (about 1.31). The D/G strength ratio of CNFs changes from 0.83 to 1.31 after the addition of GNPs, indicating that the defects in CNFs-GNPs increase. These results are in accordance with other studies [31, 43]. From Fig. 6, the observed 2D band

of GNP with a nearly symmetrical shape was centered at 2611.92 cm^{-1} , suggesting formation of single or bi-layer GNPs. Therefore, Raman spectroscopy confirms that GNP is greatly exfoliated, and the D band related to more defects occurred mostly at the edges and fractures in the GNPs. This was further proven with an FE-SEM observation. Relatively high defect graphene

nanoplates produced by the chemical method are an ideal matrix for active sites as support for electrocatalyst deposition, which can act as nucleation centers and uniform gas distribution for good management of reactions. FTIR results of GO and reduced graphene are presented in our previously published papers [27, 28].

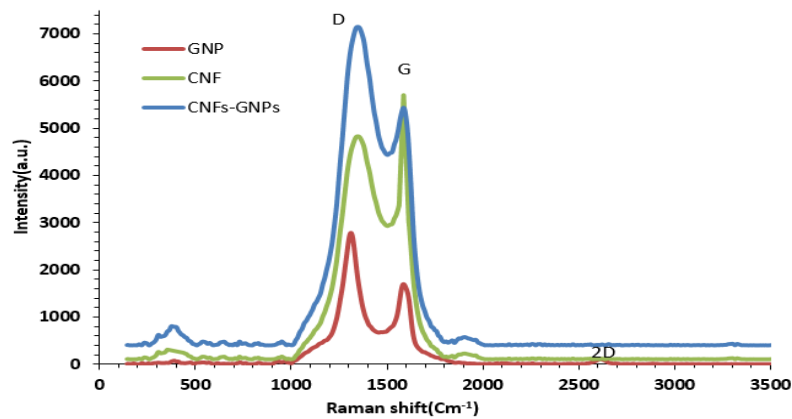


Fig. 6 .Raman spectrum of CNFs, graphene nanoplates (GNPs), and composite system of CNFs-GNPs.

Fig.7 shows the X-ray diffraction patterns of the Pt / CNFs-GNPs /GDL electrode, revealing the diffraction peaks of both carbon and platinum. The sharper and narrow diffraction peaks at $2\theta=26.49^\circ(002)$ and $54.47^\circ(004)$ are characteristic of the graphene layers and CNFs and indicate the highly graphitic and crystallinity ordered structure of these materials. Five obvious diffraction peaks were detected in the prepared Pt/CNFs-GNPs/GDL nanocomposites at 2θ values of $40.005, 46.27, 67.96, 81.64,$ and 86.66° are ascribed to face-centered cubic (fcc) facets of Pt (111), Pt (200),

Pt (220) Pt (311), and Pt (222), respectively [11, 44, 45]. Based on the Pt (111) peak on the spectrum, the mean sizes of Pt particles were estimated by the Debye-Scherrer formula (eq.1) to be 6.53 nm. This equation can be expressed as below [46]:

$$d = 0.9 \frac{\lambda}{B \cos \theta} \quad (1)$$

Where d is the diameter of the average particle size in \AA , λ is the X-ray wavelength (1.5406 \AA) for Cu, θ is the Bragg angle, and B is the full width at half maximum (fwhm) in radians.

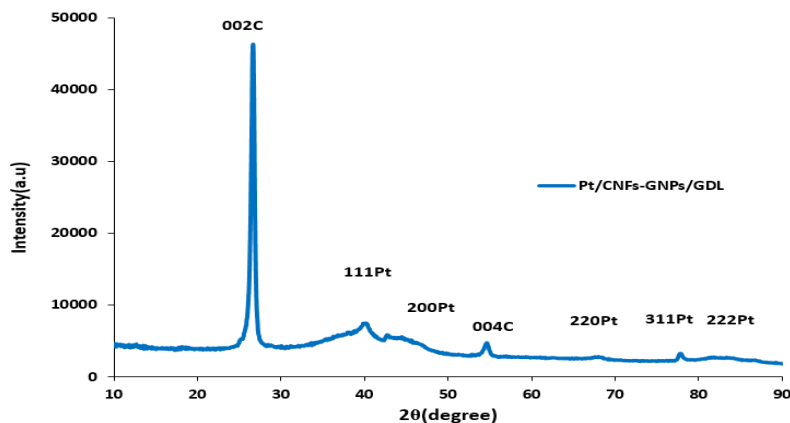


Fig .7. X-ray diffractograms of the Pt/CNFs-GNPs /GDL electrocatalyst.

3.1.2 Electrical Conductivity of Nanocomposite

The electrical conductivity of the film samples of CNFs, GNPs, and CNFs-GNPs was measured on a digital multi meter WA2017SD (Lutron). The results showed a considerable conductivity enhancement for the CNFs-GNPs composite with a value of 44.3 S/cm with respect to GNPs and CNFs with a value of 35.7 S/cm and 23.9 S/cm, respectively.

3.1.3 Specific Surface Area Measurements

The N₂ adsorption BET measurement on the prepared chemically reduced graphene oxide showed a specific surface area of 421.812 m²g⁻¹, with an average pore diameter of 2.42 nm.

3.2 Electrochemical Measurements

3.2.1 Evaluation of the Pt Deposit Characteristics from Electrochemical Measurements

The content of Pt in the composite (Pt loading) was analyzed by the electrochemical route from charge density QH calculated from the integration of the current versus time transient response. Assuming that this quantity of charge is mainly due to the faradic reaction,



The quantity of deposited Pt(mg) is obtained from the following equation [47] :

$$m_{Pt} = \frac{Q_{Pt} \cdot M_w}{n \cdot F \cdot A} \quad (3)$$

Where A is the electrode area and Mw is the molecular weight of Pt (=195.09g mol⁻¹), n=4 according to the above reaction, F=96485.309Cmol⁻¹.

Theoretically, the value of charge 350 mCcm⁻² (Fig. 2b) corresponds to a 0.16 mgcm⁻² for the Pt /CN-

Fs-GNPs/GDL catalyst. The calculation of the time necessary for metal deposition, assuming a faradic yield of 100 %, is about 36630ms, with $t_{off} = 100ms$ and $t_{on} = 10ms$ which is in good agreement with our experiments of metal deposition at the electrode surface, indicating that the faradic yield is favorable. In cases of low faradic yield, this can be related to the contribution of parasitic processes, such as double layer charging, partial reduction of Pt⁴⁺ to Pt³⁺ or Pt²⁺, and hydrogen evolution at the deposited Pt particles, which are considered negligible under the present experimental conditions. The duration of electrodeposition time was about 37s (Fig. 2a, b).

3.2.2 ECSA measurements

Fig. 8 shows typical steady-state cyclic voltammograms of Pt/C/GDL and Pt/CNFs-GNPs /GDL electrodes prepared using galvanostatic pulse electrodeposition. For cyclic voltammetry (CV) measurements, the working electrode was immersed in 0.5 M H₂SO₄ solution saturated by high purity (99.9995 %) nitrogen with the potential range between -0.24 and 1.2 V versus Ag/AgCl (saturated KCl). The scan rate was set at 50mVs⁻¹. To decrease the ohmic resistance the reference electrode was placed as close as possible to the working electrode. Before the experiment, the Nafion solution was impregnated to expand the three-dimensional reaction zones in the electrode. To determine the charge associated to the active area, CV profiles were recorded after cycling the electrode until a stationary response was obtained.

The electrochemical Pt surface areas of electrodes were calculated via the H_{upd} desorption charge, considering a conversion factor of 210 μCcm⁻² for polycrystalline Pt [48]. The electrochemical surface area (S_{ESA}), the chemical surface area (S_{CSA}), and the Pt utilization efficiency for the prepared electrocatalyst can be calculated using Eqs. 4:

$$S_{ESA} \left[\frac{m^2 Pt}{mg Pt} \right] = \frac{Q_H [\mu C cm^2]}{210 [\mu C cm^{-2} Pt] \times Ptloading [mg cm^{-2}]} \times 10^4 \quad (4)$$

Where QH is the charge for hydrogen desorption, and 210 shows the charge required for oxidation of a monolayer of H₂ on bright Pt.

$$S_{CSA} = \frac{6 \times 10^3}{\rho d} \quad (5)$$

Where ρ is the density of Pt (21.4 g cm⁻²), and d is the mean diameter of the Pt nanoparticles obtained from XRD (in nm).

From the above two areas, it is possible to estimate the Pt utilization efficiency:

$$\gamma_{Pt} = \frac{S_{ESA}}{S_{CSA}} \quad (6)$$

Table 1 presents the corresponding calculated values of S_{ESA} and γ_{Pt} .

Also, from the CV of Pt/C/GDL shown in Fig. 8, the hydrogen adsorption/desorption peaks of the Pt surface on the electrode are clearly seen, indicating the presence of polycrystalline Pt. Finally, it should be noted that no noticeable changes in the shape and nature of the Cvs of Pt/CNFs-GNPs /GDL and Pt/C/GDL electrodes were observed during the entire electrochemical measurement (after a 50-cycle pretreatment, not shown here), and the Pt real surface areas of all the catalyst kept practically constant, suggesting that the prepared catalysts are stable.

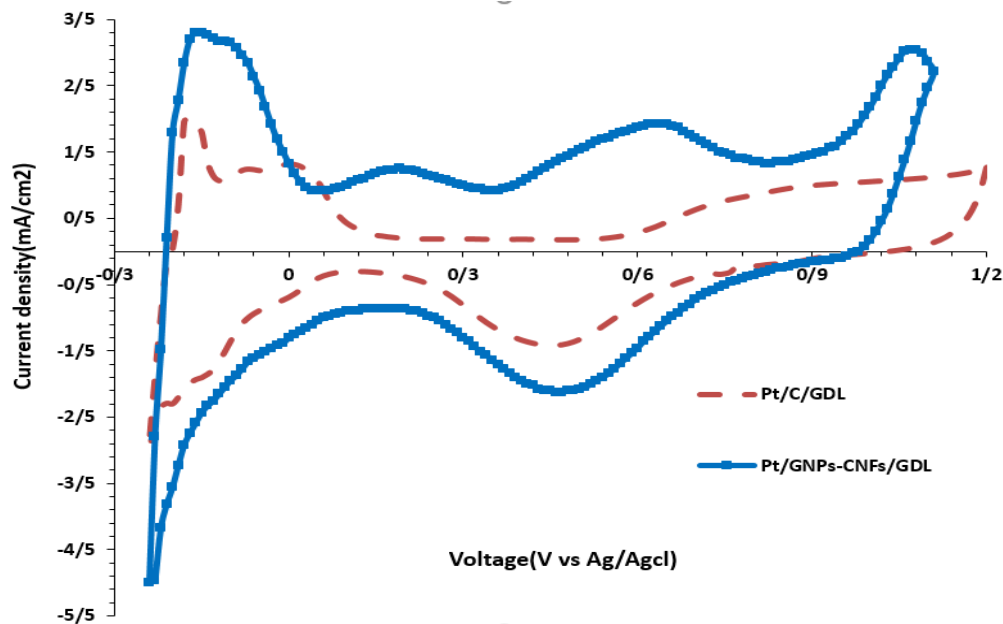


Fig.8. Cyclic voltammetry of Pt/C/carbon paper and Pt /CNFs-GNPs/carbon paper in 0.5M H₂SO₄ under continuous flowing N₂.

The electrochemical surface areas (ESA) of Pt/C/GDL and Pt/CNFs-GNPs/GDL electrodes are tabulated in Table 1. As can be seen, the Pt/CNFs-GNPs /GDL electrode had a higher Pt surface area than the Pt/C/GDL electrode. Also, the Pt/CNFs-GNPs/GDL electrode exhibits higher utilization than the Pt/C/GDL electrode. Hence, we conclude that nanoparticles in the Pt/CNFs-GNPs/GDL electrode were de-

posited preferentially on electrochemically more active sites, i.e., graphene edges (steps) and kinks. Also, CNFs edges gave rise to a strong interaction with the substrate and a definite increase in utilization efficiency. As a result, the utilization of the prepared catalysts of the Pt/GNP-CNF/GDL electrode, considering the mean particle size, is excellent (79 %) compared to the commercial one with a smaller particle size.

Table 1. Electrochemical Surface area of Pt/C/GDL and Pt/CNFs-GNPs/GDL Electrodes in N₂ Saturated Solution of 0.5M H₂SO₄.

Electrode	Pt loading ($\frac{mg}{cm^2}$)	$S_{ESA} \frac{m^2 Pt}{mg Pt}$	$S_{CSA} \frac{m^2 Pt}{mg Pt}$	γ_{Pt} (%)
Pt/C/GDL	1	28	66.75	42
Pt/CNFs-GNPs/GDL	0.16	33.34	42.93	79

3.2.3 Performance Evaluation of Catalyst through the ethanol Oxidation Reaction (EOR)

The typical cyclic voltammogram curves for ethanol electro-oxidation on Pt/CNFs-GNPs /GDL electrocatalyst recorded in 0.5 M H₂SO₄ + 1 M CH₃CH₂OH at a scan rate of 50 V s⁻¹ are shown in Fig. 9. It is well known that the activity of a catalyst is mainly evaluated by parameters of onset potential, peak potential, and current density. The voltammogram's anodic forward scan is attributed to ethanol oxidation, forming Pt-adsorbed carbonaceous species, including CO_{ads} and CH_{ads}. The backward oxidation peak is ascribed to the additional oxidation of the CO-intermediates to CO₂. In this study the ethanol oxidation began at approximately 0.50 V for Pt/CNFs-GNPs /GDL and reached its current peak at about 0.79 V. On the reverse sweep, re-oxidation of ethanol began at approximately 0.65 V and reached a peak current density at around 0.45

V, after which strongly bonded surface inter-mediate began to block the catalyst surface. The electrochemical behaviors of Pt/C were similar to that of Pt/CNFs-GNPs/GDL. However, the peak current density of Pt/CNFs-GNPs/GDL is significantly higher than Pt/C/GDL. The peak current density for Pt/CNFs-GNPs/GDL was about 1.57 mA cm⁻¹, while the peak current density for Pt/C was about 0.97 mA cm⁻¹. These facts indicate that the Pt/CNFs-GNPs /GDL have higher catalytic activity and better stability for ethanol oxidation than Pt/C/GDL because of the high electrochemical activity due to the high specific surface area of GNPs and CNFs support and high conductivity of GNPs. In addition, the observation of relatively higher I_p/I_r values on Pt/CNFs-GNPs /GDL (1.22 vs. 1.16 on Pt/C/GDL) implies that ethanol molecules are more effectively oxidized on Pt/CNFs-GNPs/GDL during the forward potential scan, generating relatively less poisoning species compared to Pt/C/GDL.

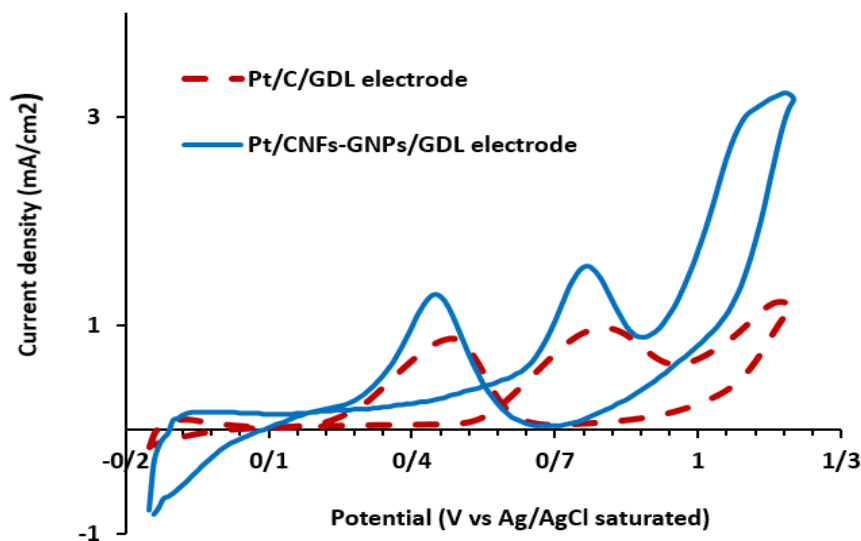


Fig.9. Cyclic voltammograms of ethanol oxidation of Pt/CNFs-GNPs/GDL and Pt/C/GDL in 0.5M H₂SO₄ + 1M C₂H₆O solution at a scan rate of 50 mVs⁻¹.

3.2.4 Linear sweep voltammetry analysis

Fig. 10 a, b shows the linear sweep voltammograms and corresponding Tafel plots for ethanol oxidation of Pt/CNFs-GNPs/GDL and Pt/C/GDL in 0.5M H₂SO₄ +1M C₂H₆O solution at a scan rate of 5 mVs⁻¹. As can be seen, the Pt/CNFs-GNPs/GDL is more active than the Pt/C/GDL electrode for ethanol electro-oxidation. The substitution of C with CNFs-GNPs

seems to improve the electrocatalytic activity of the Pt/CNFs-GNPs/GDL electrode. A Tafel slope of approximately 376 mV was measured on the Pt/C/GDL electrode and 521 mV on the Pt/CNFs-GNPs/GDL for anodic electrooxidation reaction. Also, the shape of the linear sweep voltammograms and Tafel plots obtained for the two catalysts are roughly similar, indicating that the same rate determining step occurs for the two catalysts [49, 50].

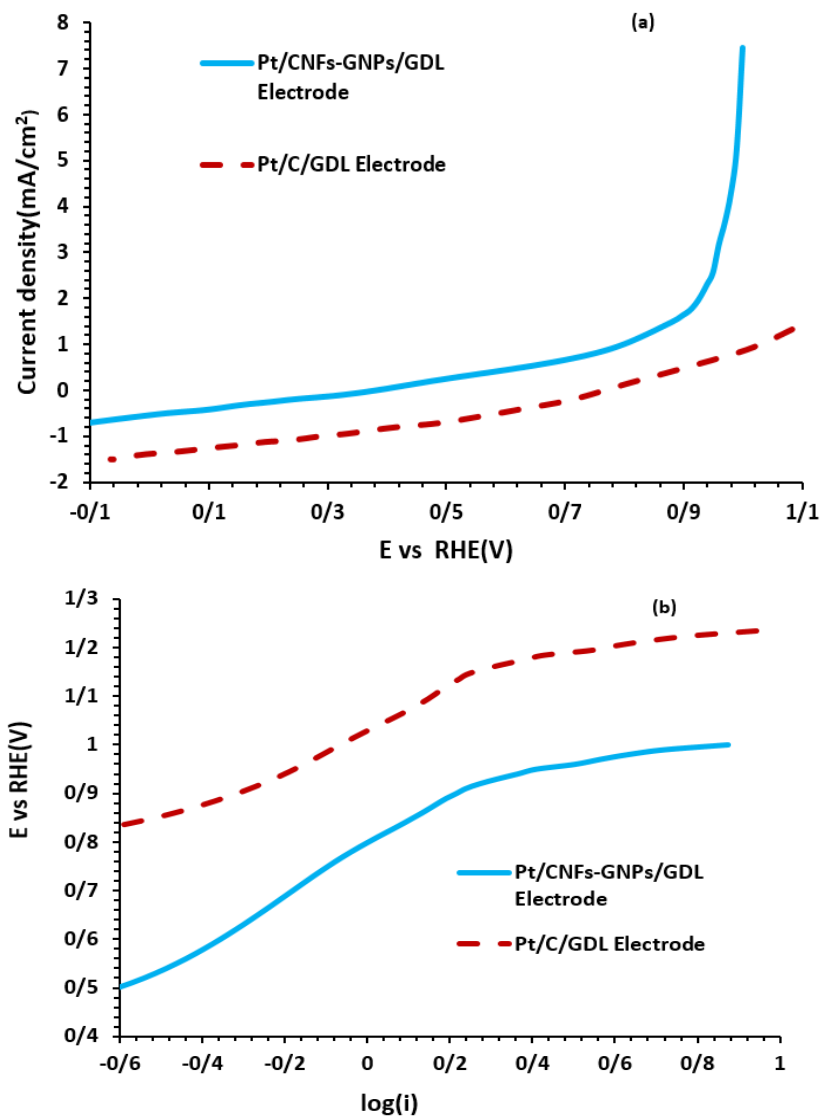


Fig.10. (a) Linear sweep voltammetry of ethanol oxidation of Pt/CNFs-GNPs/GDL and Pt/C/GDL in 0.5M H₂SO₄ +1M C₂H₆O solution at a scan rate of 55 mVs⁻¹. (b) Corresponding Tafel plots.

3.2.5 Short-term stability

Chronoamperometric experiments were performed to observe the stability and possible poisoning of the composite electrocatalyst under short-time continuous operation in 0.5M H_2SO_4 + 1M $\text{C}_2\text{H}_6\text{O}$ at 0.4V. As seen in Fig. 11, the current density of the prepared Pt/CNFs-GNPs/GDL electrode and the commercial Pt/C/GDL decayed rapidly in the initial stage, which might be due to the formation of intermediate species, such as CO_{ads} and CH_{ads} , during ethanol oxidation. However,

the current gradually reached a relatively steady state after a brief transient period. It is clear from Fig.11 that the current density for the Pt/CNFs-GNPs/GDL electrode is higher than that of Pt/C/GDL over a longer time, indicating that Pt electrodeposited on the CNFs-GNPs support can improve the electrocatalytic activity and stability of the composite. These results again confirm the high tolerance to the intermediate species and superior electrocatalytic performance of the prepared Pt/CNFs-GNPs/GDL composite catalyst in EOR.

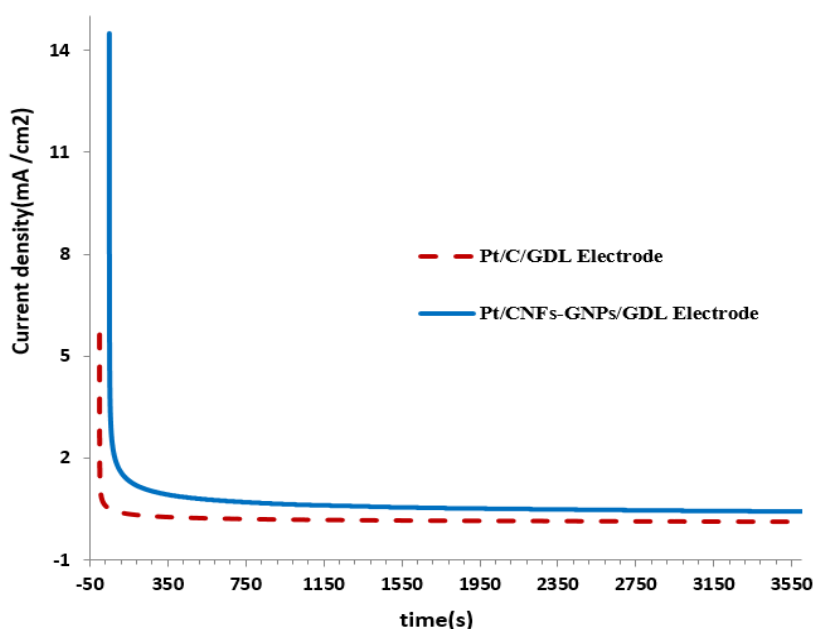


Fig. 11. Chronoamperometric curves of Pt/GNPs-CNFs/GDL and Pt/C/GDL catalysts in N_2 saturated aqueous solution of 0.5M H_2SO_4 containing 1M $\text{C}_2\text{H}_6\text{O}$ fixed potential of 0.4V for 1h. containing 1M $\text{C}_2\text{H}_6\text{O}$ fixed potential of 0.4V for 1h.

4. Conclusion

In this article, a novel CNFs-GNPs composite support material was first prepared on GDL. Then an effective strategy was used to deposit the catalyst particles on GDL using the electrochemical method. A unique mixed support was developed by layering microstructures with large porous structures of CNFs networks on its surface, as well as dense and high-conducting

GNPs networks as back supports. This unique microstructure led to improved Pt catalyst accessibility and mass exchange properties. Pt/CNFs-GNPs/GDL demonstrated promise for use as an anode electrode in DEFCs application.

References

- [1] Zhou W., Zhou Z., Song S., Li W., Sun G., Tsiakaras P. and Xin Q., "Pt based anode catalysts for direct ethanol fuel cells", *Appl.Catal.B.*, 2003,46: 273.
- [2] Song S. and Tsiakaras P., "Recent progress in direct ethanol proton exchange membrane fuel cells (DE-PEMFCs)", *Appl.Catal.B.*, 2006,63: 187.
- [3] Brandalise M., Verjullo-Silva R., Tusi M., Correa O., Farias L., Linardi M., Spinacé E. and Neto A.O., "Electro-oxidation of ethanol using PtRuBi/C electrocatalyst prepared by borohydride reduction", *Ionics*, 2009,15: 743.
- [4] Wu B., Cui R., Gao Y. and Jiang Z., "Ethanol electrocatalytic oxidation on highly dispersed Pt-TiO₂/C catalysts", *Russ. J. Electrochem*, 2009,45: 731.
- [5] Vigier F., Coutanceau C., Perrard A., Belgsir E. and Lamy C., "Development of anode catalysts for a direct ethanol fuel cell", *J. Appl. Electrochem.*, 2004,34: 439.
- [6] Neto A.O., Giz M.J.d., Perez J., Ticianelli E.A. and Gonzalez E.R., "The electro-oxidation of ethanol on Pt-Ru and Pt-Mo particles supported on high-surface-area carbon", *J. Electrochem. Soc.*, 2002,149: A272.
- [7] Rao V., Simonov P., Savinova E., Plaksin G., Cherepanova S., Kryukova G. and Stimming U., "The influence of carbon support porosity on the activity of PtRu/Sibunit anode catalysts for methanol oxidation", *J. Power Sources*, 2005,145: 178.
- [8] Alvarez G., Alcaide F., Cabot P.L., Lazaro M.J., Pastor E. and Solla-Gullon J., "Electrochemical performance of low temperature PEMFC with surface tailored carbon nanofibers as catalyst support", *Int. J. Hydrogen Energy*, 2012,37: 393.
- [9] Hacker V., Wallnöfer E., Baumgartner W., Schaffer T., Besenhard J., Schröttner H. and Schmied M., "Carbon nanofiber-based active layers for fuel cell cathodes—preparation and characterization", *Electrochem. Commun.*, 2005,7: 377.
- [10] Ji Z., Chen J., Pérez-Page M., Guo Z., Zhao Z., Cai R., Rigby M.T., Haigh S.J. and Holmes S.M., "Doped graphene/carbon black hybrid catalyst giving enhanced oxygen reduction reaction activity with high resistance to corrosion in proton exchange membrane fuel cells", *Journal of Energy Chemistry*, 2022,68: 143.
- [11] Fahrul Radzi Hanifah M., Jaafar J., Aziz M., Ismail A., Thirmizir M., Othman M., Rahman M.A. and Yusof N., "Electrocatalytic study of efficient synthesized graphene nanosheets incorporated with Pt nanoparticles for methanol oxidation reaction", *Electroanalysis*, 2016,28: 222.
- [12] Bong S., Kim Y.-R., Kim I., Woo S., Uhm S., Lee J. and Kim H., "Graphene supported electrocatalysts for methanol oxidation", *Electrochem. Commun.*, 2010,12: 129.
- [13] Zhang J., "PEM fuel cell electrocatalysts and catalyst layers: fundamentals and applications", Springer Science & Business Media. 2008,
- [14] Wang Y., Shi Z., Huang Y., Ma Y., Wang C., Chen M. and Chen Y., "Supercapacitor devices based on graphene materials", *J.Physical chem.C*, 2009,113: 13103.
- [15] SuongáOu F., "Synthesis of hybrid nanowire arrays and their application as high power supercapacitor electrodes", *Chem. Commun.*, 2008: 2373.

- [16] Wu Z.-S., Zhou G., Yin L.-C., Ren W., Li F. and Cheng H.-M., "Graphene/metal oxide composite electrode materials for energy storage", *Nano Energy*, 2012,1: 107.
- [17] Tai Z., Yan X., Lang J. and Xue Q., "Enhancement of capacitance performance of flexible carbon nanofiber paper by adding graphene nanosheets", *J. Power Sources*, 2012,199: 373.
- [18] Rakhi R. and Alshareef H.N., "Enhancement of the energy storage properties of supercapacitors using graphene nanosheets dispersed with metal oxide-loaded carbon nanotubes", *J. Power Sources*, 2011,196: 8858.
- [19] Saito T., Nishiyama Y., Putaux J.-L., Vignon M. and Isogai A., "Homogeneous suspensions of individualized microfibrils from TEMPO-catalyzed oxidation of native cellulose", *Biomacromolecules*, 2006,7: 1687.
- [20] Hajian A., Lindstrom S.B., Pettersson T., Hamedi M.M. and Wagberg L., "Understanding the dispersive action of nanocellulose for carbon nanomaterials", *Nano Lett.*, 2017,17: 1439.
- [21] Burchell T.D., "Carbon materials for advanced technologies", Elsevier, Oak Ridge, TN, USA. 1999,
- [22] Tiwari A. and Syväjärvi M., "Graphene materials: fundamentals and emerging applications", John Wiley & Sons, Hoboken, NJ, USA. 2015,
- [23] Huang H., Chen H., Sun D. and Wang X., "Graphene nanoplate-Pt composite as a high performance electrocatalyst for direct methanol fuel cells", *J. Power Sources*, 2012,204: 46.
- [24] Dong L., Gari R.R.S., Li Z., Craig M.M. and Hou S., "Graphene-supported platinum and platinum-ruthenium nanoparticles with high electrocatalytic activity for methanol and ethanol oxidation", *Carbon*, 2010,48: 781.
- [25] Yoo E., Okada T., Akita T., Kohyama M., Honma I. and Nakamura J., "Sub-nano-Pt cluster supported on graphene nanosheets for CO tolerant catalysts in polymer electrolyte fuel cells", *J. Power Sources*, 2011,196: 110.
- [26] Guo S., Dong S. and Wang E., "Three-dimensional Pt-on-Pd bimetallic nanodendrites supported on graphene nanosheet: facile synthesis and used as an advanced nanoelectrocatalyst for methanol oxidation", *ACS nano*, 2010,4: 547.
- [27] Yaldagard M., "Synthesis and electrochemical characterization of Graphene-Polyallylamine Nanocomposites as a New Supports of Pt Catalyst for Direct Methanol Fuel Cell Application", *Iranian Journal of Hydrogen & Fuel Cell*, 2019,6: 141.
- [28] Yaldagard M., "Buckypaper-based catalytic electrode containing graphene nanoplates and ZrO₂ nanorod composite to improve PEMFC performance", *Iranian Journal of Hydrogen & Fuel Cell*, 2019,5: 57.
- [29] Wang G., Shen X., Wang B., Yao J. and Park J., "Synthesis and characterisation of hydrophilic and organophilic graphene nanosheets", *Carbon*, 2009,47: 1359.
- [30] Brown B., Swain B., Hiltwine J., Brooks D.B. and Zhou Z., "Carbon nanosheet buckypaper: A graphene-carbon nanotube hybrid material for enhanced supercapacitor performance", *J. Power Sources*, 2014,272: 979.
- [31] Hou M., Xu M. and Li B., "Enhanced electrical

- conductivity of cellulose nanofiber/graphene composite paper with a sandwich structure”, *ACS Sustainable Chemistry & Engineering*, 2018,6: 2983.
- [32] Yaldagard M., Seghatoleslami N. and Jahanshahi M., “Preparation of Pt-Co nanoparticles by galvanostatic pulse electrochemical codeposition on in situ electrochemical reduced graphene nanoplates based carbon paper electrode for oxygen reduction reaction in proton exchange membrane fuel cell”, *Appl. Surf. Sci.*, 2014,315: 222.
- [33] D’Urso L., Compagnini G., Puglisi O., Scandurra A. and Cataliotti R.S., “Vibrational and photoelectron investigation of amorphous fluorinated carbon films”, *J.Physical chem.C*, 2007,111: 17437.
- [34] Park S. and Ruoff R.S., “Chemical methods for the production of graphenes”, *Nat.Nanotechnol.*, 2009,4: 217.
- [35] Stankovich S., Piner R.D., Chen X., Wu N., Nguyen S.T. and Ruoff R.S., “Stable aqueous dispersions of graphitic nanoplatelets via the reduction of exfoliated graphite oxide in the presence of poly (sodium 4-styrenesulfonate)”, *J. Mater. Chem.*, 2006,16: 155.
- [36] Stankovich S., Dikin D.A., Piner R.D., Kohlhaas K.A., Kleinhammes A., Jia Y., Wu Y., Nguyen S.T. and Ruoff R.S., “Synthesis of graphene-based nanosheets via chemical reduction of exfoliated graphite oxide”, *Carbon*, 2007,45: 1558.
- [37] Park S., An J., Jung I., Piner R.D., An S.J., Li X., Velamakanni A. and Ruoff R.S., “Colloidal suspensions of highly reduced graphene oxide in a wide variety of organic solvents”, *Nano Lett.*, 2009,9: 1593.
- [38] Hassan H.M., Abdelsayed V., Abd El Rahman S.K., AbouZeid K.M., Terner J., El-Shall M.S., Al-Resayes S.I. and El-Azhary A.A., “Microwave synthesis of graphene sheets supporting metal nanocrystals in aqueous and organic media”, *J. Mater. Chem.*, 2009,19: 3832.
- [39] Ferrari A.C., “Raman spectroscopy of graphene and graphite: disorder, electron–phonon coupling, doping and nonadiabatic effects”, *Solid State Commun.*, 2007,143: 47.
- [40] Berciaud S., Ryu S., Brus L.E. and Heinz T.F., “Probing the intrinsic properties of exfoliated graphene: Raman spectroscopy of free-standing monolayers”, *Nano Lett.*, 2008,9: 346.
- [41] Dresselhaus M.S., Jorio A., Hofmann M., Dresselhaus G. and Saito R., “Perspectives on carbon nanotubes and graphene Raman spectroscopy”, *Nano Lett.*, 2010,10: 751.
- [42] Ferrari A.C. and Robertson J., “Interpretation of Raman spectra of disordered and amorphous carbon”, *Physical review B*, 2000,61: 14095.
- [43] Lee H., Nagaishi T., Phan D.-N., Kim M., Zhang K.-Q., Wei K. and Kim I.S., “Effect of graphene incorporation in carbon nanofiber decorated with TiO₂ for photoanode applications”, *RSC advances*, 2017,7: 6574.
- [44] Hanifah M.F.R., Jaafar J., Othman M.H.D., Ismail A.F., Rahman M.A., Yusof N. and Aziz F., “An advanced, efficient and highly durable of reduced graphene oxide/platinum nanoparticles nanocomposite electrocatalyst fabricated via one-step method of the hydrothermal-assisted formic acid process for the electrocatalytic oxidation reaction of methanol”, *Solid State Sciences*, 2020,101: 106149.
- [45] Hanifah M.F.R., Jaafar J., Othman M., Ismail A.,

Rahman M., Yusof N. and Aziz F., "A novel one-step synthesis of nanocluster-like Pt incorporated reduced graphene oxide as robust nanocatalyst for highly efficient electro-catalytic oxidation of methanol", *Mater. Lett.*, 2019,254: 37.

[46] Cullity B. and Stock S., "Elements of X-ray Diffraction", Edison Wesley, London, 1978.

[47] Guo J., Tokimoto T., Othman R. and Unwin P.R., "Formation of mesoscopic silver particles at micro-and nano-liquid/liquid interfaces", *Electrochem. Commun.*, 2003,5: 1005.

[48] Pozio A., De Francesco M., Cemmi A., Cardellini F. and Giorgi L., "Comparison of high surface Pt/C catalysts by cyclic voltammetry", *J. Power Sources*, 2002,105: 13.

[49] Yu E.H., Scott K. and Reeve R.W., "A study of the anodic oxidation of methanol on Pt in alkaline solutions", *J. Electroanal. Chem.*, 2003,547: 17.

[50] Bai Y., Wu J., Xi J., Wang J., Zhu W., Chen L. and Qiu X., "Electrochemical oxidation of ethanol on Pt-ZrO₂/C catalyst", *Electrochem. Commun.*, 2005,7: 1087.